Chemistry–A European Journal

Research Article
doi.org/10.1002/chem.202201738

Check for updates

Europe
European Chemical
Societies Publishing

www.chemeurj.org

Reaction of Pertechnetate in Highly Alkaline Solution: Synthesis and Characterization of the Nitridotrioxotechnetate Ba[TcO₃N]

D. Badea,[a] K. Dardenne,[b] R. Polly,[b] J. Rothe,[b] M. Hanrath,[a] M. Reimer,[a] K. Meerholz,[a] J.-M. Neudörfl,[a] E. Strub,[a] and J. Bruns*[a]

Abstract: The preparation of novel technetium oxides, their characterization and the general investigation of technetium chemistry are of significant importance, since fundamental research has so far mainly focused on the group homologues. Whereas the structure chemistry of technetium in strongly oxidizing media is dominated by the $[TcO_4]^-$ anion, our recent investigation yielded the new $[TcO_3N]^{2-}$ anion. Brown single crystals of Ba[TcO₃N] were obtained under hydrothermal conditions starting from $Ba(OH)_2 \cdot 8H_2O$ and $NH_4[TcO_4]$ at 200 °C. Ba[TcO₃N] crystallizes in the monoclinic crystal system with the space group $P2_1/n$ ($a = 7.2159(4)$ Å, $b = 7.8536(5)$ Å, $c = 7.4931(4)$ Å and $\beta = 104.279(2)°$). The crystal structure of Ba[TcO₃N] consists of isolated $[TcO_3N]^{2-}$ tetrahedra, which are surrounded by Ba^{2+} cations. XANES measurements complement the oxidation state +VII for technetium and Raman spectroscopic experiments on Ba[TcO₃N] single crystals exhibit characteristic Tc—O and Tc—N vibrational modes.

Introduction

^{99}Tc is a long-lived fission product of ^{235}U accumulated in reprocessing residues upon the extraction of plutonium from irradiated uranium fuel rods. For each ton of spent nuclear fuel, technetium is formed in the order of kilograms.[1] Therefore, it is essential to study the chemistry of technetium – especially with respect to its possible behavior in long-term storage facilities.

Due to the fact that working with technetium and its compounds requires a radionuclide laboratory, the majority of publications on fundamental technetium chemistry dates from the 1950s to the 1970s.[2] Today's research is mainly concentrated on ^{99}Tc, due to the medical importance of this isotope.[3] About 40 million medical examinations are performed annually using ^{99m}Tc.[4] In a radioactive waste repository, ^{99}Tc becomes one of the most important radionuclides after plutonium on a timescale of about 50,000 years.[5] In contrast to Pu, the chemistry of technetium is scarcely investigated.

Current studies on the long-lived isotope ^{99}Tc are mostly limited to the work of a few research groups, since working with the radioelement requires enhanced safety precautions.[6] Considering the current fields of research, it is notable that the behavior of technetium during spent fuel reprocessing and in the environment has been investigated intensively by using acidic solutions.[7] However, only a few publications with regard to technetium in alkaline media are known.[8] For instance, the products from the radiolysis of the pertechnetate $[TcO_4]^-$ in highly alkaline solutions were investigated.[8c,9] As another example, the oxidation states of technetium in alkaline solutions were determined by electrochemical reduction reactions.[10] Fundamental research has been resumed to reexamine the reaction of sulfide with pertechnetate in alkaline solutions.[6b] However, the fundamental understanding of Tc redox chemistry in alkaline media is also important in the context of nuclear waste, since alkaline conditions prevail in some high level waste tanks.[8a] Thus, the removal of $[TcO_4]^-$ from highly alkaline legacy defense nuclear tank waste was studied.[8b,d]

In this work, the reaction of ammonium pertechnetate in a highly alkaline $Ba(OH)_2$ medium was investigated. The obtained barium nitridotrioxotechnetate(VII) Ba[TcO₃N] was successfully synthesized and characterized. In addition to the crystal structure analysis, XAFS (XANES and EXAFS) and Raman experiments were performed. The experimental data has been complemented by computational studies.

[a] D. Badea, Dr. M. Hanrath, M. Reimer, Prof. Dr. K. Meerholz, Dr. J.-M. Neudörfl, Dr. E. Strub, Dr. J. Bruns
Department of Chemistry
University of Cologne
Greinstr. 4–6, 50939 Cologne (Germany)
E-mail: j.bruns@uni-koeln.de
Homepage: www.agbruns-iac.uni-koeln.de

[b] Dr. K. Dardenne, Dr. R. Polly, Dr. J. Rothe
Institute for Nuclear Waste Disposal
Karlsruhe Institute of Technology
Hermann-von-Helmholtz-Platz 1, 76344 Eggenstein-Leopoldshafen (Germany)

Supporting information for this article is available on the WWW under https://doi.org/10.1002/chem.202201738

Chem. Eur. J. 2022, e202201738 (1 of 7)

© 2022 The Authors. Chemistry - A European Journal published by Wiley-VCH GmbH

Chemistry–A European Journal

Research Article
doi.org/10.1002/chem.202201738

Chemistry Europe
European Chemical
Societies Publishing

Results and Discussion

Single crystals of barium nitridotrioxotechnetate(VII) Ba[TcO$_3$N] were obtained under highly alkaline conditions using NH$_4$[TcO$_4$] and Ba(OH)$_2\cdot$8H$_2$O in water at 200°C. Figure 1 shows a picture of a Ba[TcO$_3$N] single crystal positioned in a glass capillary.

The title compound crystallizes in the monoclinic crystal system with the space group $P2_1/n$. Crystallographic data for the refined structure is given in Table 1. The crystal structure consists of discrete [TcO$_3$N]$^{2-}$ tetrahedra, which are charge compensated by Ba^{2+} cations (Figure 2). The latter are surrounded by oxygen and nitrogen atoms in a distorted bicapped square antiprismatic fashion (Figure 3).
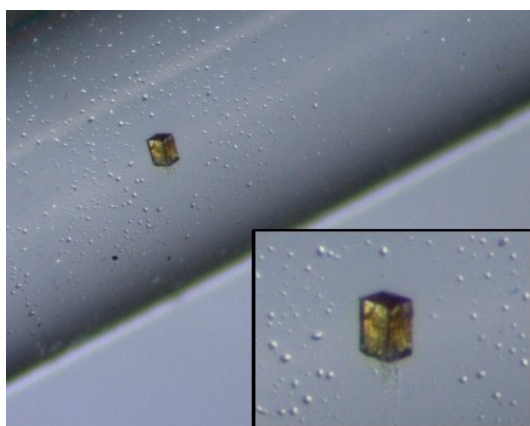

Figure 1. Microscopic picture of a single crystal of Ba[TcO$_3$N] positioned in a glass capillary.

Table 1. Crystal and structure refinement data for Ba[TcO$_3$N].

Empirical formula	Ba[TcO$_3$N]
Formula weight	297.35
Temperature	100(2) K
Wavelength	1.54178 Å
Crystal system	monoclinic
Space group	$P2_1/n$
Unit cell dimensions	$a = 7.2159(4)$ Å
	$b = 7.8536(5)$ Å $\beta = 104.279(2)°$
	$c = 7.4931(4)$ Å
Volume	411.52(4) Å^3
Z	4
Density (calculated)	4.799 g cm^{-3}
F(000)	520
Crystal size	0.02×0.02×0.01 mm^3
2θ range for data collection	15.27° to 144.08°
Index ranges	$-8 \leq h \leq 8,\ -9 \leq k \leq 9,\ -9 \leq l \leq 9$
Reflections collected	6998
Independent reflections	810 [$R_{int} = 0.0627$]
Completeness to theta	99.7%
Absorption correction	multi-scan
Maximum/minimum transmission	0.0092/0.0853
Data/restraints/parameters	810/0/56
Goodness-of-fit on F^2	1.116
Final R indices [$I > 2$sigma(I_o)]	$R_1 = 0.0375$, $wR_2 = 0.0952$
R indices (all data)	$R_1 = 0.0401$, $wR_2 = 0.0955$
Largest diff. peak and hole	2.46/-1.13 e Å^{-3}
CCDC number	2176571

The structure contains one distinct technetium, nitrogen and barium atom, respectively. However, three crystallographically distinguishable oxygen atoms are found.

The technetium atom is coordinated by three oxygen atoms, exhibiting Tc—O bond lengths of 1.763(4) Å, 1.776(4) Å and 1.777(4) Å. The fourth technetium-ligand bond within the tetrahedron is significantly shorter, exhibiting a length of 1.692(5) Å and thus giving hint for a Tc—N bond. Accordingly, the formation of the nitridotrioxotechnetate anion can be assumed. Apart from the new [TcO$_3$N]$^{2-}$ anion, only a small number of other nitridotrioxometallates, such as K$_2$[ReO$_3$N], M[OsO$_3$N] (M = K, Rb, Ag, Cs, Tl), Ba$_2$[VO$_3$N] and Ba$_3$[WO$_3$N]$_2$, are known.[11] Even though some of the nitridotrioxometallates have already been synthesized, still not all of them have been structurally elucidated by single crystal X-ray diffraction.[11] Ba$_3$[WO$_3$N]$_2$ was synthesized by heating Ba$_3$W$_2$O$_9$ at high temperatures in the range of 700°C in a stream of NH$_3$ gas.[11e] K[OsO$_3$N] can be obtained through milder reaction conditions starting from OsO$_4$, KOH and NH$_4$OH, whereas the other nitrodotrioxoosmates are synthesized by reacting the potassium salt with slightly soluble salts of the cations in aqueous solution.[11c] By the use of liquid ammonia, K$_2$[ReO$_3$N] has been prepared from the reaction of potassium amide with rhenium heptoxide.[11b] In the case of Ba[TcO$_3$N], an OH$^-$ assisted ammonolysis to insert the nitrogen atom according to the following reaction equations can be assumed:

$$OH^- + NH_4^+ \rightarrow NH_3 + H_2O \tag{1}$$

$$[TcO_4]^- + NH_3 + OH^- \rightarrow [TcO_3N]^{2-} + 2H_2O \tag{2}$$
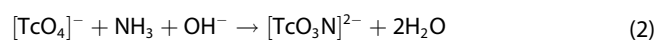
The reaction is quite similar to the synthesis of K[OsO$_3$N], making OH$^-$ assisted ammonolysis an efficient way for the insertion of nitrogen into oxometallates. In case of technetium's lighter and heavier homologues Mn and Re, the same reactions have not been successful. However, radiolytic effects can be excluded, since they have not been observed in any of our previous experimental studies with ^{99}Tc, even when dealing with macroscopic amounts of TcO$_2$(s) in solubility experiments.[12]

In addition to the performed single crystal X-ray experiments, the structure of Ba[TcO$_3$N] was optimized with DFT calculations. The calculated unit cell is shown in Figure 4. The optimized values comply excellently with the experimental data shown in Table S3 in the Supporting Information. The calculated values of the cell parameters $a = 7.32$ Å, $b = 8.00$ Å and $c = 7.62$ Å agree with the available structural data $a = 7.2159(4)$ Å, $b = 7.8536(5)$ Å and $c = 7.4931(4)$ Å. Furthermore, the lengths of 1.69 Å and 1.78 Å for the Tc—N and Tc—O bonds, which are in excellent agreement with the experimental results, were determined (see Table S3 for the other calculated distances as well). Figure 5 shows the DFT-optimized structures and schematical MO of tetrahedral pertechnetate [Tc(VII)O$_4$]$^-$ and [Tc(VII)O$_3$N]$^{2-}$ in the gas phase.

The optimization of the [Tc(VII)O$_3$N]$^{2-}$ anion in the gas phase in C$_{3v}$ symmetry yields similar results with 1.71 Å and 1.79 Å for the Tc—N and Tc—O distances, respectively. Hence,
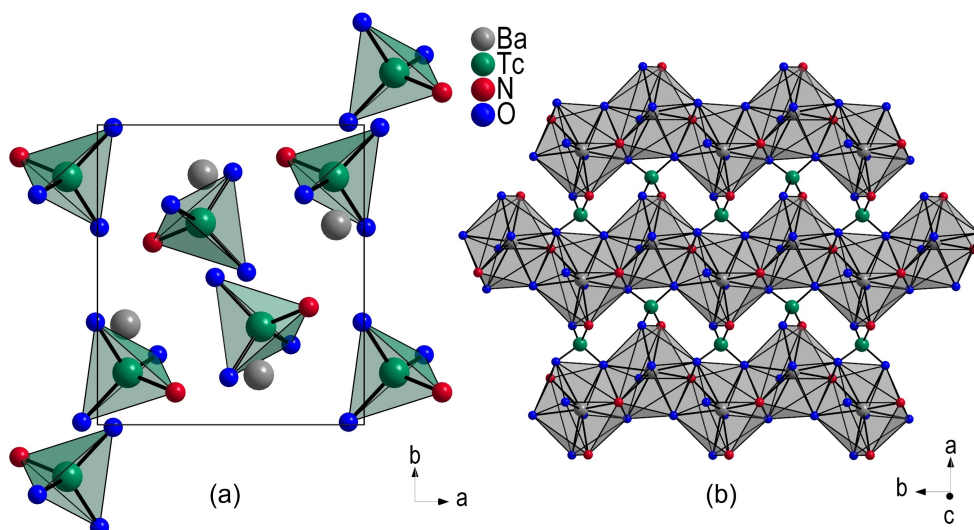
Chemistry–A European Journal

Research Article
doi.org/10.1002/chem.202201738

Chemistry
Europe
European Chemical
Societies Publishing

Figure 2. a) Crystal structure of Ba[TcO$_3$N] with the representation of the unit cell; b) coordination polyhedra of Ba^{2+} extending in the *a-b* plane.
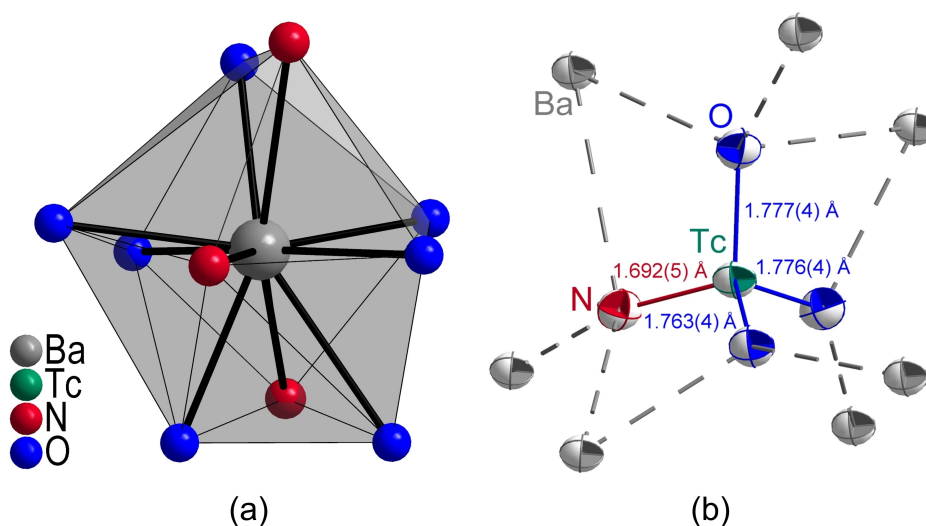

Figure 3. a) Coordination geometry around the barium cation and b) ellipsoid representation of the [TcO$_3$N]$^{2-}$ anion with coordinating Ba^{2+} cations. The thermal ellipsoids are drawn with a probability of 70%.
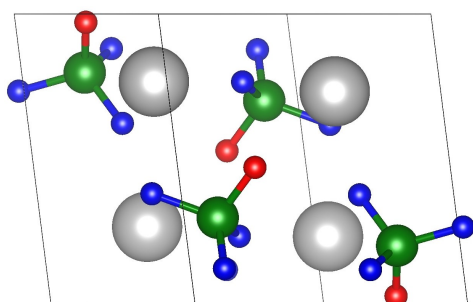

Figure 4. Unit cell of the optimized Ba[TcO$_3$N] structure; color code: grey-barium, blue-oxygen, red-nitrogen, green-technetium.

both approaches result in very similar structures of the [Tc-(VII)O$_3$N]$^{2-}$ species.

In addition to structural studies of Ba[TcO$_3$N], Raman spectroscopic experiments using a Renishaw inVia Raman microscope were performed on exactly the same single crystal which has been used for SCXRD. Figure 6 shows the Raman spectrum of Ba[TcO$_3$N]. The prominent bands are observed between 986 and 299 cm^{-1}.

In comparison with the spectra of [OsO$_3$N]$^-$ and by the use of quantum chemical calculations, the bands of [TcO$_3$N]$^{2-}$ have been assigned.[11e,13] The calculated Raman and IR spectrum are given in the Supporting Information together with a detailed assignment of the respective vibrations (Figures S2, S3 and Table S7 in the Supporting Information). Accordingly, the strong absorption band at 986 cm^{-1} belongs to the Tc–N stretching
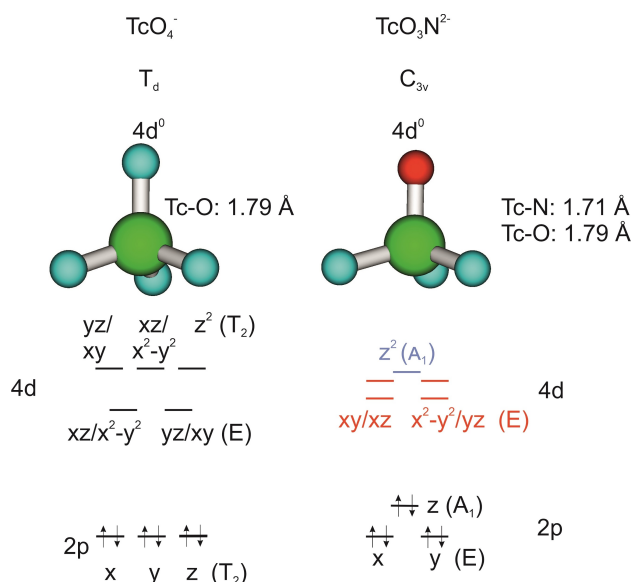
Chem. Eur. J. **2022**, e202201738 (3 of 7)

© 2022 The Authors. Chemistry - A European Journal published by Wiley-VCH GmbH

Chemistry–A European Journal

Research Article
doi.org/10.1002/chem.202201738

Chemistry Europe
European Chemical
Societies Publishing

Figure 5. DFT-optimized structures (in the gas phase) and schematic MO of a) tetrahedral pertechnetate $[Tc(VII)O_4]^-$, b) $[Tc(VII)O_3N]^{2-}$ in C_{3v} symmetry.

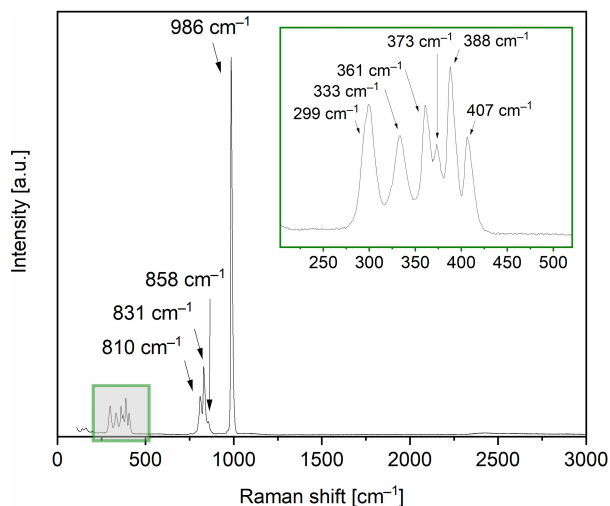**Figure 6.** Raman spectrum of Ba[TcO₃N] with a cutout for better clarity.

vibration. The less intense bands at 858, 831, 810 cm^{-1} can be attributed to Tc–O stretching modes. The bands between 407 and 361 cm^{-1} stem from O–Tc–N bending vibrations and those at 333 and 299 cm^{-1} from O–Tc–O bending vibrations.

To determine the valence state of technetium, X-ray absorption near edge structure (XANES) spectroscopy studies of the title compound were conducted at the Tc K- and L_3-edges along with corresponding measurements of $[Tc(VII)O_4]^-$ species in aqueous solution ([Tc] = 20 mM obtained by dissolution of Na[TcO₄] in 0.1 M HCl) as a reference. In comparison to studies on the Tc K-edge, this is only the fifth known L_3-edge XANES measurement performed with a technetium sample.[14] Additionally, relativistic multi-reference ab initio calculations were applied to calculate the Tc L_3-edge XANES spectra of both

compounds. The calculated spectra for both optimized gas phase structures, shown in Figure 7, are almost identical. This is also the case for the corresponding experimental Tc L_3-XANES spectra of $[Tc(VII)O_3N]^{2-}$ and $[Tc(VII)O_4]^{2-}$ shown in Figure 7, right hand side. Note that the absolute energy positions between calculated and experimental spectra are off by more than 20 eV, indicating a systematic uncertainty in the determination of the Fermi level by the applied theory.

For the $[Tc(VII)O_3N]^{2-}$ anion, the Tc–N bond is oriented along the z-axis. As the ground state has an empty 4d shell (S = 0), it is a single reference closed shell state. Since spin-orbit (SO) effects are important, all relevant excited singlet and triplet states, fifteen each, were determined in the calculations. From the MO diagram in Figure 5 it is evident that the energy of excited states with an electron occupying a mixed $4d_{\pm\pi}/4d_{\pm\delta}$ ($4d_{xz}/4d_{yz}/4d_{xy}/4d_{x2-y2}$) orbital (in the irreducible representation E) is lower compared to states with an $4d_\sigma$ ($4d_{z2}$) occupation (in the irreducible representation A_1), because $4d_\sigma$ points directly towards the nitrogen atom with the Tc–N distance shorter compared to the Tc–O distances. Hence, there are more peaks to be expected compared to $[Tc(VII)O_4]^-$.

Due to the ligand field splitting of the 4d orbitals in C_{3v}, there are two lower lying states in the irreducible representation E of C_{3v} and one higher lying state in A_1 (see Figure 5). The two peaks visible in the spectrum (denoted as 1 and 2 in Figure 7) can be assigned to excitations from $2p_{3/2} \rightarrow 4d_{yz}/4d_{x2-y2}$, $4d_{xy}/4d_{xz}$ (all 4d orbitals in E) and $2p_{3/2} \rightarrow 4d_{z2}$ (4d orbitals in A_1), respectively. The excited states are predominantly singlet states (S = 0). The splitting between the two peaks is ~2.3 eV for the RASSCF calculations, being very close to the experimental value of 2.0 eV. Moreover, Figure 8 depicts the comparison of the Tc K-edge XANES spectra (corresponding to dipole-allowed 1 s→5p excitations) obtained for both Tc compounds. Note that the distinct pre-edge peak above 21.050 eV generally indicates the presence of a tetrahedral pertechnetate $(Tc(VII)O_4^-)$-like Tc bonding environment. The absence of an inversion center allows for the hybridization of the transition metal's 4d and 5p states, thus rendering the lowest laying unoccupied electronic states accessible for Tc 1s core electrons (cf.[14a] and references therein). This coordination structure is as well reflected by Tc K EXAFS of the title compound compared to aqueous pertechnetate moieties (structural parameters and spectra obtained from EXAFS are shown in Table S5 and Figure S1 in the Supporting Information). Thus, the Tc oxidation state of +VII in Ba[TcO₃N] has not only been proven indirectly by the detection of Tc–N bands in the Raman spectrum, but also directly by means of Tc K/L_3-edge XAFS spectroscopy and multireference ab initio calculations of Tc L_3-edge XANES spectra.

Conclusion

Since technetium is formed in order of kilograms for each ton of spent nuclear fuel, technetium redox chemistry as well as its behaviour in long-term storage facilities needs to be investigated. Hitherto, there is a significant lack in knowledge about
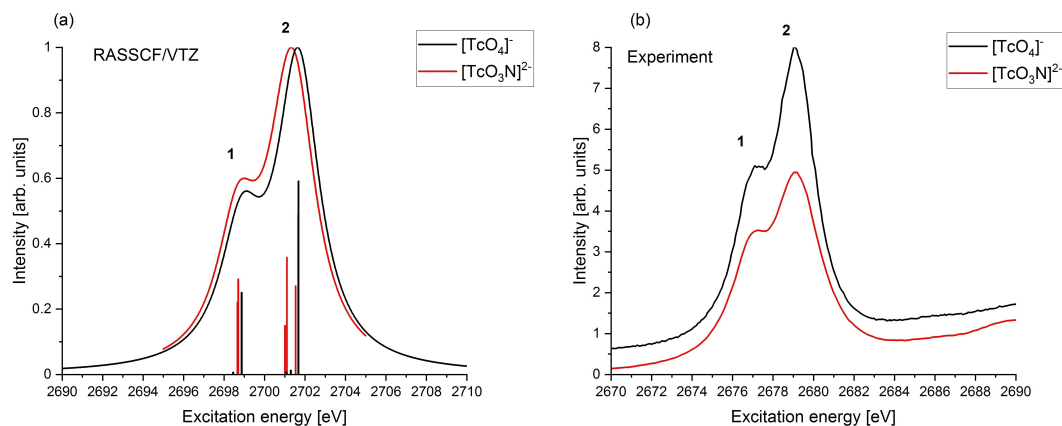
Chemistry–A European Journal

Research Article
doi.org/10.1002/chem.202201738

Chemistry Europe
European Chemical
Societies Publishing

Figure 7. (a) ab initio Tc L_3-edge XANES spectra of $[Tc(VII)O_3N]^{2-}$ ($[Tc(VII)O_4]^-$ shown for comparison) obtained by RASSCF/ANO-VTZ calculations based on the DFT gas phase structure optimization (see Figure 5), vertical bars representing transition energies and oscillator strengths of relevant Tc $2p_{3/2} \rightarrow 4d_{5/2}$ excitations and spectral envelopes (solid lines) obtained by convoluting bars with Lorentzians. (b) Normalized Tc L_3-edge XANES spectra of $[Tc(VII)O_3N]^{2-}$ and $[Tc(VII)O_4]^-$ (the latter one vertically shifted for clarity).
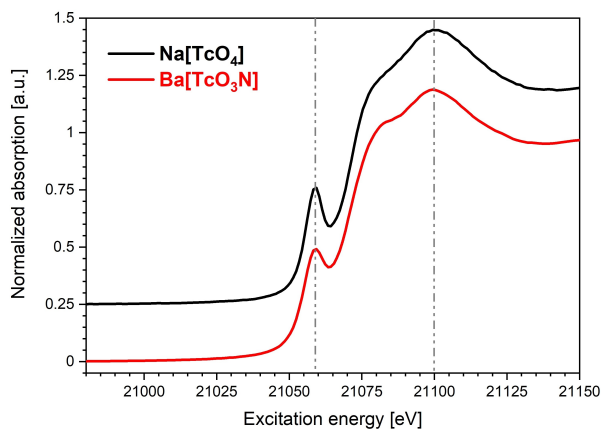
Figure 8. Normalized Tc K-edge XANES spectra of $[Tc(VII)O_3N]^{2-}$ and $[Tc(VII)O_4]^-$ (the latter one vertically shifted for clarity).

the behaviour of technetium species in alkaline media. With the synthesis of Ba[TcO₃N] from barium hydroxide, water and ammonium pertechnetate, the stability of the Tc oxidation state +VII even under as harsh conditions, as for example highly concentrated alkaline solution, can be underlined. It might occur in a final repository for nuclear waste in geological salt formations, for example, in case of the degradation of cementitious waste forms. The oxidation state has been proven by detailed XANES and EXAFS investigations, which have been corroborated by quantum chemical calculation.

From a preparative viewpoint, the introduced reaction of an OH⁻ assisted ammonolysis is an easy and energetically favourable way for the insertion of nitrogen into oxoanions for future reactions. Since so far only one nitrogen per technetium atom has been introduced, further experiments are planned to increase the nitrogen content per technetium atom by adding excess ammonium hydroxide in stoichiometric amounts.

Experimental Section

Caution! ^{99}Tc is a β^- emitter. All operations have to be done in a specially equipped radiochemical laboratory. Appropriate shielding has to be employed during all manipulations of ^{99}Tc containing samples.

Synthesis: Brown single crystals of Ba[TcO₃N] were obtained from a barium hydroxide octahydrate solution by applying hydrothermal conditions using a Teflon-lined stainless steel autoclave. A typical batch contained 5.4 mg NH₄[TcO₄] (*Oak Ridge National Laboratory*, purity not specified), 63.7 mg Ba(OH)₂·8H₂O (*Alfa Aesar*, 98%) and 63.7 mL H₂O. The reagents were combined in a Teflon beaker and subsequently heated in a stainless steel autoclave at 200 °C for 10 h. After decreasing the temperature within 30 h to room temperature, the crystals of the title compound were obtained in a colorless matrix. The product formation is highly dependent on the used amount of water and Ba(OH)₂·8H₂O, so that even small changes prevent successful reaction. For the afore mentioned batch size at least 100 crystals were obtained. They were all of roughly uniform shape and color. The single crystals were removed from the flux mechanically. Removal of the flux to obtain a phase pure bulk material was neither successful by washing with water nor with methanol or other solvents. However, the crystal color and habitus remained unchanged after washing with water and methanol.

Single crystal X-ray diffraction: Single crystal XRD data were collected on a Bruker D8 Venture using Cu-K$_\alpha$ radiation ($\lambda =$ 1.54178 Å), an X-ray optics mirror and a Photon III detector. The crystal was prepared under a polarization microscope and measured at reduced temperature. The lattice parameters, the refinement details, the atomic parameters and selected bond lengths are given in Tables S1–S4 in the Supporting Information. The structure solution and refinement was successful using ShelXL/ShelXT in Olex2.[15] The pictures of the structure were developed with the Diamond program.[16]

Deposition Number(s) 2176571 contain(s) the supplementary crystallographic data for this paper. These data are provided free of charge by the joint Cambridge Crystallographic Data Centre and Fachinformationszentrum Karlsruhe Access Structures service.

Raman spectroscopy: Single crystals of the title compound were selected in glass capillaries and placed under a Renishaw inVia

Raman microscope. The spectra were recorded with a 532 nm laser excitation at room temperature.

Tc K/L₃-edge XAFS spectroscopy: X-ray absorption fine structure (XAFS) measurements were performed at the Tc K-edge (E_{1s} (Tc⁰) = 21.044 keV, Tc 1s→5p transitions, including extended X-ray absorption fine structure, EXAFS) and at the Tc L₃-edge ($E_{2p3/2}$ (Tc⁰) = 2.677 keV, Tc 2p$_{3/2}$→4d transitions, only covering the X-ray absorption near edge structure, XANES). The K- and L₃-edge spectra in the hard and 'tender' X-ray regime, respectively, were recorded at the INE-Beamline[17] of the KIT Light Source (KARA storage ring, KIT Campus North) in total fluorescence yield detection mode. Details of the data acquisition procedures have been recently reported elsewhere.[14a] At the Tc K-edge, Ba[TcO₃N] crystals were accumulated in the tip of sealed polyethylene vials installed in an Ar-flushed flow-through sample holder. At the L₃-edge, the ground crystals were measured dispersed on adhesive KAPTON® (polyimide) film covered by a thin (13 μm) KAPTON foil. The resulting pouches were installed in the He-flushed low energy sample chamber described in Ref. [14a].

Quantum chemical calculations

Relativistic multireference ab initio study of Tc L₃-XANES spectra: Recently, relativistic multiconfiguration ab initio quantum chemistry methods have developed into a powerful tool supporting X-ray spectroscopy techniques.[18] Because of the complexity of the detected signals, theoretical calculations are mandatory for the interpretation of the experimental data. For recent extensive reviews see, for example.[19]

Structures of the [Tc(VII)O₃N]²⁻ species: The calculation of the XANES spectra of [Tc(VII)O₃N]²⁻ requires reliable structures. The structure of [Tc(VII)O₃N]²⁻ was optimized with Density Functional Theory (DFT).[20] For the gas phase structure the RI-DFT method was used as available in TURBOMOLE (www.turbomole.com)[21] employing the def2-TZVP[22] basis set. Additionally, the crystal structure of the nitridotrioxotechnetate Ba[TcO₃N] was optimized with DFT based on periodic boundary conditions as implemented in the Vienna Ab Initio Simulation Package (VASP).[23] The Kohn-Sham equations were solved using a plane-wave basis set. Electron exchange and correlation were described using the Perdew-Burke-Ernzerhof (PBE) version[24] of the generalized gradient approximation (GGA). The core electrons were described by projector augmented wave (PAW) potentials[25] as implemented by Kresse and Joubert.[26] For the calculations an energy cutoff of E_{cut} = 500 eV was chosen. The resulting *xyz* coordinates are given in Table S6.

Tc L₃-XANES calculations: The calculation of the Tc L₃-XANES spectra (corresponding to 2p$_{3/2}$→4d$_{3/2,5/2}$ excitations) of the [Tc(VII)O₃N]²⁻ were carried out as outlined in Ref. [27] using relativistic multireference ab initio methods available in MOLCAS8.4.[28] The restricted active space (RASSCF) method[29] was used for the calculation of Spin-orbit interactions (SO) in the restricted-active-space state-interaction (RASSI) scheme.[30] For the RASSCF calculations the active space was subdivided. The RAS1 space contains the three 2p orbitals and the five 4d orbitals occupy the RAS3 space. In total six active electrons are distributed in the active space. Both scalar relativistic and spin-orbit coupling (SOC) were accounted for in our calculations. For the spin-orbit interaction calculations all relevant spin states were included in the calculations. The ANO-VTZ basis set available in MOLCAS was used.[31] The calculations were performed using the full C₃ᵥ symmetry with the SUPERSYMMETRY option imposing higher supersymmetry by restricting rotations to irreducible representations in the RASSCF calculations. Experimental spectra were simulated by applying a Lorentzian profile at the calculated

transition energies with the intensities given by the oscillator strengths with a full width at half maximum of $\gamma = 2.5$ eV for the different species.

Vibrational spectroscopy calculation: Additionally, solid state calculations with the CRYSTAL program suite[32] using pob-TZVP[33] (Ba, O, N) and ERD_2017 (Tc) basis sets and PBESol[34] and HSESol[35] density functional theory were carried out. All optimized geometries were confirmed by subsequent frequency calculations. Intensities were obtained for the PBESol functional using CRYSTAL's CPKS[36] module. In order to achieve convergence all calculations were conducted in internal coordinates with the XXL integration grid.

IR and Raman frequencies were calculated using CRYSTAL[37] within the harmonic approximation (Table S7). The simulated Raman and IR spectra were calculated using the PBESol functional only since CRYSTAL does not allow for the calculation of intensities for the HSESol functional. However, we cross checked the locations of the transitions with the HSESol functional and found no significant difference. Obtained normal modes were analyzed by visual inspection and classified as stretching, bending or skeletal modes. For visualization of the spectra, calculated Raman and IR intensities were fitted with Lorentzian functions (Figures S2 and S3).

Acknowledgements

Conflict of Interest

The authors declare no conflict of interest.

Data Availability Statement

The data that support the findings of this study are available in the supplementary material of this article.

[1] M. Y. Khalil, W. B. White, *J. Am. Ceram. Soc.* **1983**, *66*, 197–198.

[2] a) J. W. Cobble, W. T. Smith, G. E. Boyd, *J. Am. Chem. Soc.* **1953**, *75*, 5777–5782; b) R. H. Colton, R. D. Peacock, *Q. Rev. Chem. Soc.* **1962**, *16*, 299–315; c) A. A. Pozdnyakov, *Russ. Chem. Rev.* **1965**, *34*, 129–141.

[3] a) C. Gallini, F. Tutino, R. Martone, A. Ciaccio, E. N. Costanzo, G. Taborchi, S. Morini, S. Bartolini, S. Farsetti, C. Di Mario, F. Perfetto, F. Cappelli, *J. Nucl. Cardiol.* **2021**, *28*, 90–99; b) K. Koyanagawa, M. Naya, T. Aikawa, O. Manabe, M. Kuzume, H. Ohira, I. Tsujino, N. Tamaki, T. Anzai, *J. Nucl. Cardiol.* **2021**, *28*, 128–136; c) K. V. Zavadovsky, A. V. Mochula, A. A. Boshchenko, A. V. Vrublevsky, A. E. Baev, A. L. Krylov, M. O. Gulya, E. A. Nesterov, R. Liga, A. Gimelli, *J. Nucl. Cardiol.* **2021**, *28*, 249–259.

[4] W. C. Eckelman, *J. Am. Coll. Cardiol.* **2009**, *2*, 364–368.

[5] P. N. Swift, D. Sassani, *Impacts of Nuclear Fuel Cycle Choices on Permanent Disposal of High-Activity Radioactive Wastes.* **2019**, No.
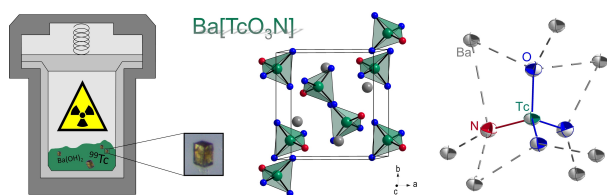
Chemistry–A European Journal

Research Article
doi.org/10.1002/chem.202201738

Chemistry Europe
European Chemical
Societies Publishing

SAND2019-5941 C. Sandia National Lab.(SNL-NM), Albuquerque, NM (United States), 2019.

[6] a) R. Alberto, *J. Organomet. Chem.* **2018**, *869*, 264–269; b) N. Edelstein, C. Burns, D. Shuh, W. Lukens, *Research Program to Investigate the Fundamental Chemistry of Technetium*, **2000**; c) F. Poineau, E. E. Rodriguez, P. F. Weck, A. P. Sattelberger, P. Forster, T. Hartmann, E. Mausolf, G. W. C. Silva, G. D. Jarvinen, A. K. Cheetham, K. R. Czerwinski, *J. Radioanal. Nucl. Chem.* **2009**, *282*, 605–609.

[7] a) N. D. Goletskii, B. Y. Zilberman, Y. S. Fedorov, A. S. Kudinov, A. A. Timoshuk, L. V. Sytnik, E. A. Puzikov, S. A. Rodionov, A. P. Krinitsyn, V. I. Ryazantsev, D. V. Ryabkov, *Radiochemistry* **2014**, *56*, 501–514; b) M. Lin, I. Kajan, D. Schumann, A. Türler, *J. Radioanal. Nucl. Chem.* **2019**, *322*, 1857–1862; c) M. Zegke, D. Grödler, M. Roca Jungfer, A. Haseloer, M. Kreuter, J. M. Neudörfl, T. Sittel, C. M. James, J. Rothe, M. Altmaier, A. Klein, M. Breugst, U. Abram, E. Strub, M. S. Wickleder, *Angew. Chem. Int. Ed.* **2022**, *61*, e202113777.

[8] a) W. W. Lukens, D. K. Shuh, N. C. Schroeder, K. R. Ashley, in *226 American Chemical Society Meeting*, United States, **2003**; b) J. Li, B. Li, N. Shen, L. Chen, Q. Guo, L. Chen, L. He, X. Dai, Z. Chai, S. Wang, *ACS Cent. Sci.* **2021**, *7*, 1441–1450; c) W. W. Lukens, J. J. Bucher, N. M. Edelstein, D. K. Shuh, *Environ. Sci. Technol.* **2002**, *36*, 1124–1129; d) N. Shen, Z. Yang, S. Liu, X. Dai, C. Xiao, K. Taylor-Pashow, D. Li, C. Yang, J. Li, Y. Zhang, M. Zhang, R. Zhou, Z. Chai, S. Wang, *Nat. Commun.* **2020**, *11*, 5571.

[9] W. W. Lukens, J. J. Bucher, N. M. Edelstein, D. K. Shuh, *J. Phys. Chem. A* **2001**, *105*, 9611–9615.

[10] M. Chotkowski, M. Grdeń, B. Wrzosek, *J. Electroanal. Chem.* **2018**, *829*, 148–156.

[11] a) S. J. Clarke, P. R. Chalker, J. Holman, C. W. Michie, M. Puyet, M. J. Rosseinsky, *J. Am. Chem. Soc.* **2002**, *124*, 3337–3342; b) B. Krebs, A. Müller, *J. Inorg. Nucl. Chem.* **1968**, *30*, 463–466; c) A. Müller, F. Bollmann, *Z. Naturforsch. B* **1968**, *23*, 1539–1539; d) R. Pastuszak, P. L'Haridon, R. Marchand, Y. Laurent, *Acta Crystallogr. Sect. B* **1982**, *38*, 1427–1430; e) P. Subramanya Herle, M. S. Hegde, G. N. Subbanna, *J. Mater. Chem.* **1997**, *7*, 2121–2125.

[12] a) T. Kobayashi, A. C. Scheinost, D. Fellhauer, X. Gaona, M. Altmaier, *Radiochim. Acta* **2013**, *101*, 323–332; b) E. Yalçıntaş, X. Gaona, A. C. Scheinost, T. Kobayashi, M. Altmaier, H. Geckeis, *Radiochim. Acta* **2015**, *103*, 57–72; c) E. P. Yalcintas, X. Gaona, M. Altmaier, K. Dardenne, R. Polly, H. Geckeis, *Dalton Trans.* **2016**, *45*, 8916–8936; d) A. Baumann, E. Yalcintas, X. Gaona, R. Polly, K. Dardenne, T. Prüßmann, J. Rothe, M. Altmaier, H. Geckeis, *Dalton Trans.* **2018**, *47*, 4377–4392.

[13] A. Müller, E. J. Baran, F. Bollmann, P. J. Aymonino, *Z. Naturforsch.* **1969**, *24*, 960–964.

[14] a) K. Dardenne, S. Duckworth, X. Gaona, R. Polly, B. Schimmelpfennig, T. Pruessmann, J. Rothe, M. Altmaier, H. Geckeis, *Inorg. Chem.* **2021**, *60*, 12285–12298; b) P. E. R. Blanchard, E. Reynolds, B. J. Kennedy, C. D. Ling, Z. Zhang, G. Thorogood, B. C. C. Cowie, L. Thomsen, *J. Synchrotron Radiat.* **2014**, *21*, 1275–1281; c) S. Bauters, A. C. Scheinost, K. Schmeide, S. Weiss, K. Dardenne, J. Rothe, N. Mayordomo, R. Steudtner, T. Stumpf, U. Abram, S. M. Butorin, K. O. Kvashnina, *Chem. Commun.* **2020**, *56*, 9608–9611.

[15] a) O. V. Dolomanov, L. J. Bourhis, R. J. Gildea, J. A. K. Howard, H. Puschmann, *J. Appl. Crystallogr.* **2009**, *42*, 339–341; b) G. Sheldrick, *Acta Crystallogr. Sect. C* **2015**, *71*, 3–8.

[16] K. Brandenburg, *Diamond 4, Crystal and Molecular Structure Visualization*, Crystal Impact GbR, Bonn, Germany, **2019**.

[17] J. Rothe, S. Butorin, K. Dardenne, M. A. Denecke, B. Kienzler, M. Löble, V. Metz, A. Seibert, M. Steppert, T. Vitova, C. Walther, H. Geckeis, *Rev. Sci. Instrum.* **2012**, *83*, 043105.

[18] a) I. Josefsson, K. Kunnus, S. Schreck, A. Föhlisch, F. de Groot, P. Wernet, M. Odelius, *J. Phys. Chem. Lett.* **2012**, *3*, 3565–3570; b) R. V. Pinjari, M. G. Delcey, M. Guo, M. Odelius, M. Lundberg, *J. Phys. Chem. Lett.* **2015**, *142*, 069901; c) R. V. Pinjari, M. G. Delcey, M. Guo, M. Odelius, M. Lundberg, *J. Comput. Chem.* **2016**, *37*, 477–486.

[19] a) P. Norman, A. Dreuw, *Chem. Rev.* **2018**, *118*, 7208–7248; b) S. I. Bokarev, O. Kühn, *Wiley Interdiscip. Rev.: Comput. Mol. Sci.* **2020**, *10*, e1433; c) M. Lundberg, M. G. Delcey, in *Transition Metals in Coordination Environments*, 1 ed., Springer International Publishing, Cham, Schwitzerland, **2019**, pp. 185–217.

[20] a) P. Hohenberg, W. Kohn, *Phys. Rev.* **1964**, *136*, B864–B871; b) W. Kohn, L. J. Sham, *Phys. Rev.* **1965**, *140*, A1133–A1138.

[21] a) A. Schäfer, H. Horn, R. Ahlrichs, *J. Chem. Phys.* **1992**, *97*, 2571–2577; b) K. Eichkorn, O. Treutler, H. Öhm, M. Häser, R. Ahlrichs, *Chem. Phys. Lett.* **1995**, *240*, 283–290; c) O. Treutler, R. Ahlrichs, *J. Chem. Phys.* **1995**, *102*, 346–354; d) K. Eichkorn, F. Weigend, O. Treutler, R. Ahlrichs, *Theor. Chem. Acc.* **1997**, *97*, 119–124; e) M. v. Arnim, R. Ahlrichs, *J. Chem. Phys.* **1999**, *111*, 9183–9190; f) P. Deglmann, K. May, F. Furche, R. Ahlrichs, *Chem. Phys. Lett.* **2004**, *384*, 103–107.

[22] a) F. Weigend, M. Häser, H. Patzelt, R. Ahlrichs, *Chem. Phys. Lett.* **1998**, *294*, 143–152; b) F. Weigend, R. Ahlrichs, *Phys. Chem. Chem. Phys.* **2005**, *7*, 3297–3305; c) D. Andrae, U. Häußermann, M. Dolg, H. Stoll, H. Preuß, *Theor. Chim. Acta* **1990**, *77*, 123–141.

[23] a) G. Kresse, J. Hafner, *Phys. Rev. B* **1993**, *48*, 13115–13118; b) G. Kresse, J. Furthmüller, *Phys. Rev. B* **1996**, *54*, 11169–11186; c) G. Kresse, J. Furthmüller, *Comput. Mater. Sci.* **1996**, *6*, 15–50.

[24] J. P. Perdew, K. Burke, M. Ernzerhof, *Phys. Rev. Lett.* **1996**, *77*, 3865–3868.

[25] P. E. Blöchl, *Phys. Rev. B* **1994**, *50*, 17953–17979.

[26] G. Kresse, D. Joubert, *Phys. Rev. B* **1999**, *59*, 1758–1775.

[27] a) K. Dardenne, S. Duckworth, X. Gaona, R. Polly, B. Schimmelpfennig, T. Pruessmann, J. Rothe, M. Altmaier, H. Geckeis, *Inorg. Chem.* **2021**, *60*, 12285–12298; b) R. Polly, B. Schacherl, J. Rothe, T. Vitova, *Inorg. Chem.* **2021**, *60*, 18764–18776.

[28] F. Aquilante, J. Autschbach, R. K. Carlson, L. F. Chibotaru, M. G. Delcey, L. De Vico, I. Fdez. Galván, N. Ferré, L. M. Frutos, L. Gagliardi, M. Garavelli, A. Giussani, C. E. Hoyer, G. Li Manni, H. Lischka, D. Ma, P. Å. Malmqvist, T. Müller, A. Nenov, M. Olivucci, T. B. Pedersen, D. Peng, F. Plasser, B. Pritchard, M. Reiher, I. Rivalta, I. Schapiro, J. Segarra-Martí, M. Stenrup, D. G. Truhlar, L. Ungur, A. Valentini, S. Vancoillie, V. Veryazov, V. P. Vysotskiy, O. Weingart, F. Zapata, R. Lindh, *J. Comput. Chem.* **2016**, *37*, 506–541.

[29] P. A. Malmqvist, A. Rendell, B. O. Roos, *J. Phys. Chem.* **1990**, *94*, 5477–5482.

[30] P.-Å. Malmqvist, B. Roos, B. Schimmelpfennig, *Chem. Phys. Lett.* **2002**, *357*, 230–240.

[31] a) B. O. Roos, R. Lindh, P.-Å. Malmqvist, V. Veryazov, P.-O. Widmark, *J. Phys. Chem. A* **2004**, *108*, 2851–2858; b) B. O. Roos, R. Lindh, P.-Å. Malmqvist, V. Veryazov, P.-O. Widmark, *J. Phys. Chem. A* **2005**, *109*, 6575–6579.

[32] R. Dovesi, R. Orlando, A. Erba, C. Zicovich-Wilson, B. Civalleri, S. Casassa, L. Maschio, M. Ferrabone, M. De La Pierre, P. D'arco, M. Rérat, B. Kirtman, *Int. J. Quantum Chem.* **2014**, *114*, 1287–1317.

[33] a) M. F. Peintinger, D. V. Oliveira, T. Bredow, *J. Comput. Chem.* **2012**, *34*, 451–459; b) D. Vilela Oliveira, J. Laun, M. F. Peintinger, T. Bredow, *J. Comput. Chem.* **2019**, *40*, 2364–2376.

[34] J. P. Perdew, A. Ruzsinszky, G. I. Csonka, O. A. Vydrov, G. E. Scuseria, L. A. Constantin, X. L. Zhou, K. Burke, *Phys. Rev. Lett.* **2008**, *100*, 136406-1-136406-4.

[35] L. Schimka, J. Harl, G. Kresse, *J. Chem. Phys.* **2011**, *134*, 024116-1-024116-11.

[36] a) M. Ferrero, M. Rérat, B. Kirtman, R. Dovesi, *J. Chem. Phys.* **2008**, *129*, 244110; b) M. Ferrero, M. Rérat, R. Orlando, R. Dovesi, *J. Comput. Chem.* **2008**, *29*, 1450–1459; c) M. Ferrero, M. Rérat, R. Orlando, R. Dovesi, *J. Chem. Phys.* **2008**, *128*, 014110.

[37] a) F. Pascale, C. M. Zicovich-Wilson, F. López Gejo, B. Civalleri, R. Orlando, R. Dovesi, *J. Comput. Chem.* **2004**, *25*, 888–897; b) C. M. Zicovich-Wilson, F. Pascale, C. Roetti, V. R. Saunders, R. Orlando, R. Dovesi, *J. Comput. Chem.* **2004**, *25*, 1873–1881.

RESEARCH ARTICLE

Ba[TcO₃N]

D. Badea, Dr. K. Dardenne, Dr. R. Polly,
Dr. J. Rothe, Dr. M. Hanrath, M. Reimer,
Prof. Dr. K. Meerholz, Dr. J.-M. Neudörfl,
Dr. E. Strub, Dr. J. Bruns*

Reaction of Pertechnetate in Highly Alkaline Solution: Synthesis and Characterization of the Nitridotrioxotechnetate Ba[TcO₃N]

Hot chemistry. The nitridotrioxotechnetate anion has been obtained by the reaction of ammonium pertechnetate under highly alkaline conditions. In addition to a single crystal structure analysis, Raman data proves the existence of Tc—O and Tc—N bonds. The oxidation state $+$VII has further been corroborate by XANES and EXAFS measurements.